Journal of Nuclear Medicine, published on October 25, 2019 as doi:10.2967/jnumed.119.232488

Multimodality Imaging of Inflammation and Ventricular Remodeling in Pressure Overload Heart Failure

Aylina Glasenapp,[1,2] Katja Derlin,[2] Yong Wang,[3] Marion Bankstahl,[4] Martin Meier,[4] Kai C Wollert,[3] Frank M Bengel,[1] James T Thackeray[1]

Departments of [1]Nuclear Medicine, [2]Radiology, and [3]Cardiology and Angiology;

[4]Central Laboratory Animal Facility and Institute for Laboratory Animal Science

Hannover Medical School, Hannover, Germany

Short title: FDG imaging of inflammation after TAC

Word Count: 4487

First Author
Aylina Glasenapp, Department of Radiology,
Hannover Medical School, Carl Neuberg Str 1, 30625 Hannover, Germany

Corresponding Author
James T Thackeray, PhD
Department of Nuclear Medicine
Hannover Medical School
Carl Neuberg Str 1
30625 Hannover
Germany
+49 511/532.3358
thackeray.james@mh-hannover.de

Inflammation contributes to ventricular remodeling after myocardial ischemia, but its role in non-ischemic heart failure is poorly understood. Local tissue inflammation is difficult to assess serially during pathogenesis. While ^{18}F-fluorodeoxyglucose (FDG) accumulates in inflammatory leukocytes which may identify inflammation in the myocardial microenvironment, it remains unclear whether this imaging technique can isolate diffuse leukocytes in pressure overload heart failure. We aimed to evaluate the capability to serially image inflammation with 18F-FDG in the early stages of pressure overload-induced heart failure, and to compare the timecourse to functional impairment assessed by cardiac magnetic resonance imaging (MRI). **Methods.** C57Bl6/N mice underwent transverse aortic constriction (TAC, n=22) or sham surgery (n=12), or coronary ligation as an inflammation-positive control (n=5). MRI assessed ventricular geometry and contractile function at d2 and d8 after TAC. Immunostaining identified the extent of inflammatory leukocyte infiltration early in pressure overload. ^{18}F-FDG PET scans were acquired at d3 and d7 after TAC, under ketamine-xylazine anesthesia to suppress cardiomyocyte glucose uptake. **Results.** Pressure overload evokes rapid left ventricular dilation compared to sham (end systolic volume, d2: 40.6±10.2μL vs. 23.8 ±1.7μL, $p<0.001$). Contractile function was similarly impaired (ejection fraction, d2: 40.9 ± 9.7% vs. 59.2 ± 4.4%, $p<0.001$). Severity of contractile impairment was proportional to histology-defined myocardial macrophage density at d8 ($r=-0.669$; $p=0.010$). Positron emission tomography (PET) imaging identified significantly higher ^{18}F-FDG accumulation in the left ventricle of TAC compared to sham mice at d3 (10.5±4.1%ID/g vs. 3.8±0.9%ID/g, $p<0.001$) and at d7 (7.8±3.7%ID/g vs.3.0 ±0.8%ID/g $p=0.006$), though the efficiency of cardiomyocyte suppression was variable between TAC mice. The ^{18}F-FDG signal correlated to ejection fraction ($r = -0.75$, $p=0.01$)

and ventricle volumes (r=0.75, p<0.01). Western immunoblotting demonstrated 60% elevation of myocardial glucose transporter 4 expression in the left ventricle at d8 after TAC, indicating altered glucose metabolism. **Conclusion.** TAC induces rapid changes in left ventricle geometry and contractile function, with a parallel modest infiltration of inflammatory macrophages. Metabolic remodeling overshadows inflammatory leukocyte signal using 18F-FDG PET imaging. More selective inflammatory tracers are requisite to selectively identify the diffuse local inflammation in pressure overload.

Key words: Heart failure, PET, ^{18}F-FDG, inflammation, MRI, macrophage

INTRODUCTION

Heart failure (HF) is a multifactorial syndrome and the common endpoint of many cardiovascular diseases. Despite improvements in early treatment strategies, HF remains a prevalent cause of death worldwide and a significant burden on the healthcare system (*1*). Conventional therapeutic approaches combine multiple drugs targeting nonspecific symptoms and common mechanisms of HF, to support cardiac function and improve survival (*2*). But various specific pathogenetic mechanisms contributing to development and progression of HF remain undertreated, particularly in non-ischemic heart failure (*3*). Recent evidence suggests that inflammatory leukocytes and macrophages may play a role in non-ischemic HF progression (*4*), and contribute to interstitial fibrosis and contractile dysfunction (*4*). HF patients exhibit elevated circulating white blood cells, inflammatory cytokines and biomarkers, regardless of pathogenesis (*5,6*). As such, inflammation has emerged as a potential therapeutic target for not only ischemic heart failure, but also non-ischemic cardiomyopathies (*7*).

Acute infiltration of inflammatory leukocytes predicts functional decline and progression of HF following ischemic injury (*8*). Conversely, inflammatory cell infiltration and adverse ventricular remodeling in non-ischemic pressure overload is less well characterized, but the temporal dynamics and involved cell population are thought to be distinct from ischemic injury (*9*). At 7d after aortic banding, total macrophages and leukocyte content of the left ventricle is maximal (*10-12*), and may contribute to ventricular remodeling (*13,14*). While systemic inflammation may be quantified through biomarkers or leukocyte count, local myocardial inflammatory activity is more difficult to assess. Positron

emission tomography (PET) using ^{18}F-deoxyglucose (^{18}F-FDG) robustly accumulates in activated inflammatory leukocytes including macrophages (*15*). In the myocardium, however, this is complicated by physiologic uptake of FDG into viable myocytes, which is further enhanced by ischemia or other injury (*16*). Acute pressure overload instigates rapid changes in myocyte glucose metabolism, which is believed to contribute to ventricular hypertrophy (*17,18*). Nevertheless, inflammation-targeted ^{18}F-FDG imaging, using preparation protocols for suppression of myocyte uptake, has demonstrated prognostic value for outcomes after myocardial infarction in patients and animal models (*8,19*). But the feasibility of imaging myocardial inflammation in non-ischemic heart failure is undefined.

We hypothesized that ^{18}F-FDG PET imaging would identify infiltrating macrophages and inflammatory leukocytes in the myocardium early in the pathogenesis of non-ischemic pressure overload-induced HF. Accordingly, we compared the uptake of ^{18}F-FDG in the left ventricle after transverse aortic constriction in mice (using a myocyte uptake suppression protocol) to the progressive changes in left ventricle geometry and contractile function assessed by cardiac magnetic resonance imaging (MRI). This was complemented by histological and biochemical tissue workup to determine factors underlying the imaging signal.

METHODS

Animals

All animal experiments were approved by the state authority (Niedersächsisches Landesamt für Verbraucherschutz und Lebensmittelsicherheit) and local animal ethics

review. Male C57Bl/6N mice (n=39, 23.7±1.5g) were purchased from Charles River (Sulzfeld, Germany) and housed in groups in a temperature-controlled facility under a 14h/10h light/dark cycle with food and water freely available.

Transverse aortic constriction (TAC)

Mice underwent TAC (n=22) or sham surgery (n=12) under isoflurane anesthesia, as described previously (*20*). Briefly, mice were pretreated with analgesic carprofen (5mg/kg sc) and anesthetized by isoflurane (induction 3-4%, 3L/min oxygen; maintained 1.5-2% after oral intubation under mechanical ventilation). Atropine sulfate (0.05mg/kg, sc) prevented bradycardia and tracheal mucus accumulation. A lateral thoracotomy in the second intercostal space was performed and the thymus gently retracted. The aorta was exposed by blunt dissection and gently separated from surrounding tissue between the brachiocephalic trunk and the left carotid artery. To constrict the transverse aorta, a 6-0 silk suture was secured around the vessel using a blunt 25G needle to define a consistent ligature diameter. After securing the suture, the needle was removed, the rib cage and skin closed, and the animal allowed to recover before returning to the home cage. For sham operation, the identical procedure was followed without securing the suture. Following surgery, oral analgesia was maintained with Tramadol (2.5mg/100ml in drinking water).

Myocardial infarction (MI)

As a positive control that exhibits robust macrophage infiltration, MI was induced by coronary artery ligation as described (*21*). Briefly, mice (n=5) pretreated with butorphanol analgesic (2mg/kg sc) were anaesthetized with isoflurane (induction at 3-4%, 3L/min oxygen; maintained at 1.5-2% after oral intubation under mechanical ventilation).

Left thoracotomy was performed and the left anterior descending coronary artery was permanently ligated.

Study Design

Ventricular geometry and contractile function early in pressure overload heart failure was assessed by cardiac MRI at d2 and d8 after surgery. Inflammation was serially assessed by ^{18}F-FDG positron emission tomography (PET) under ketamine-xylazine anesthesia to suppress cardiomyocyte glucose uptake at d3 and d7 after surgery. These imaging timepoints were selected based on the expected maximal inflammatory cell infiltration (d7) based on flow cytometry studies (*10,14*), with an intermediate timepoint to allow evaluation of changes over the first week after TAC. All mice were killed by cervical dislocation at d8-9 for ex vivo tissue workup. An additional group was killed at d3 for histologic workup. ^{18}F-FDG images were acquired at d3 after surgical MI, which evokes robust inflammatory cell infiltration of the infarct territory.

Histopathology

Mice were killed at d3 (n=4) after TAC or after MI (n=1) and at d8 (n=8) after TAC or after sham surgery (n=8), for histologic assessment of inflammation. Hearts were removed, cleaned in phosphate buffered saline, and frozen under optimal cutting temperature compound (Tissue Tek). Adjacent long axis 10μm sections were sliced using a cryostat (Shandon) and thaw-mounted onto charged slides (Superfrost Plus). Immunostaining for CD68 and Ly6G identified macrophages and granulocytes, respectively.

Small animal magnetic resonance imaging

Mice (TAC n=10, sham n=4) underwent MRI at 2d and 8d after surgery using a 7 Tesla small animal MRI system (Pharmascan 70/16, Bruker BioSpin GmbH, Ettlingen, Germany; Software ParaVision 6.0.1). Cardiac function and geometry were evaluated by using a navigator-based self-gated cine MRI sequence (IntraGate FLASH, Bruker Biospin, Ettlingen, Germany) as described previously (*22*).

MR image analysis

Image analysis was performed with CVI (Vers. 5.3.6) to determine ventricle volumes and assess heart function. Endocardial and epicardial contours were defined on short axis sections and used to calculate ventricular mass at end systole and end diastole; ejection fraction was calculated from endocardial volumes.

Small animal positron emission tomography

Mice (TAC n=10, sham n=4; MI n=5) underwent PET imaging using a dedicated small animal PET camera (Inveon DPET, Siemens), as previously described (*21*). Briefly, mice were anesthetized with ketamine (84mg/kg ip) / xylazine (11.2mg/kg ip) to suppress glucose uptake by cardiomyocytes (*21*), and positioned prone on the imaging bed with the heart centered in the scanner field of view. ^{18}F-FDG (12.7±0.9 MBq) was administered as a 0.15mL bolus through a lateral tail vein catheter. A 60 min dynamic listmode PET scan. ^{18}F-FDG was synthesized using standard kits and production methods. One mouse died between the first and second PET acquisitions.

PET Image Analysis

Images were dynamically histogrammed and reconstructed using iterative OSEM3D/MAP as described previously (*21*). Analysis was performed with Inveon Research Workplace 4.2 (Siemens Medical Solutions USA) to evaluate left ventricular volume and signal. A region of interest (ROI) was defined on the left ventricle myocardium by interactive thresholding as previously described (*21*). Size and position of the ROI was verified by anatomic landmarks in the fused CT images. The signal was evaluated semi-quantitatively as percent injected dose per gram of tissue (%ID/g). Additional details are provided in the online supplement.

Western Immunoblotting

Hearts from a subset of animals (TAC n=4, sham n=4) were processed for immunoblotting using lysates of left and right ventricle. Additional details are provided in the online supplement.

Statistics

Statistical analysis was conducted using Prism 6 (GraphPad). All data are shown as mean ± SD. Serial imaging data obtained in individual animals were compared using Student's paired t-test. TAC and sham groups were compared using the Welch t-test for unequal variance. Pearson product-moment correlation coefficients described the relationship between pairs of continuous variables. $P < 0.05$ was considered statistically significant.

RESULTS

Pressure Overload Evokes Early Left Ventricular Dilation and Cardiac Dysfunction

Within 2d of TAC, cardiac MRI demonstrated 30% increase in left ventricle mass and a corresponding elevation in ventricular volumes compared to sham (Fig. 1A). Ventricular mass was consistently elevated in the first week after TAC surgery (d2: 87.5±14.6 mg vs. 66.3±8.4mg, p=0.007; d8: 89.3±7.8mg vs. 67.3±9.5mg, p=0.010) (Fig. 1B). Similarly, a progressive increase in end systolic volumes and end diastolic volumes were identified from 2 and 8d post-surgery (ESV d2: 40.6±10.2μL vs. 23.8 ±1.7μL, p<0.001; d8: 47.2±11.1μL vs. 17.8±3.1 p<0.001) (EDV d2: 68.5±7.2μL vs. 58.5 ±2.4μL, p=0.002; d8: 75.4±9.9 vs. 56.3±5.9, p=0.002) compared to sham (Fig. 1B). TAC animals exhibited a marked reduction in ejection fraction at 2d (40.9 ± 9.7% vs. 59.2 ± 4.4%, p<0.001) and 8d post-surgery (37.5 ± 11.8 vs. 68.3±3.4, p<0.001) compared to sham (Fig. 1B), consistent with early and persistently impaired contractile function after pressure overload.

Left Ventricle Macrophage Infiltration Correlates with Contractile Dysfunction

To investigate myocardial inflammation, CD68- and Ly6G immunostaining identified inflammatory leukocyte infiltration. CD68-positive macrophages were noted throughout the left ventricle after TAC, at a diffuse density compared to myocardial infarction (Fig. 2A). Semi-quantification of cell infiltration revealed a threefold elevation of CD68+ cells in the left ventricle of TAC mice compared to sham at d3 and twice as many cells at d8 (d3: 111.9±61.8 cells/field, p=0.094; d8: 74.4 ± 24.3 cells/field, p=0.003; vs. sham: 37.6 ± 11.2 cells/field) (Fig. 2B). Macrophage density after TAC was much lower compared to extensive staining after MI, where quantitative calculation is complicated by the large abundance of

CD68+ staining (Fig. 2A). Nevertheless, in TAC and sham mice, the CD68 cell count inversely correlated with ejection fraction (r=-0.669; p=0.010) (Fig. 2B), suggesting a relationship between inflammatory cell infiltration and functional decline. Ly6G-positive granulocytes were present but at lower density than macrophages after TAC (Supplemental Fig. 1).

Myocardial ^{18}F-FDG Signal under Ketamine-Xylazine (K/X) Suppression is Elevated after TAC

K/X anesthesia significantly lowered cardiomyocyte ^{18}F-FDG uptake in sham operated animals to background levels (<5%ID/g) (Supplemental Fig. 2). In inflammation positive control MI mice, cardiomyocyte uptake of ^{18}F-FDG was effectively suppressed, with global myocardial PET signal <10%ID/g, and a hotspot localized to the infarct territory, consistent with histology findings (Fig. 3A). By contrast, TAC-operated animals exhibited a range of modest to robust ^{18}F-FDG accumulation throughout the left ventricle, despite significantly lower inflammatory cell content. The left ventricular ^{18}F-FDG uptake in TAC operated mice exceeded that of MI at 3d (8/10 mice) and at 7d (4/9 mice), suggesting ineffective cardiomyocyte suppression despite identical K/X protocol (Supplemental Fig. 3). Semi-quantitative analysis confirmed higher ^{18}F-FDG signal in the left ventricle of TAC mice compared to sham at d3 (+176%, 10.5±4.1%ID/g vs. 3.8±0.9%ID/g, p<0.001) and at d7 (+160%, 7.8±3.7%ID/g vs.3.0 ±0.8%ID/g p=0.006) (Fig. 3B). The inconsistency of the PET signal localization and intensity necessitated further interrogation of the source of this ^{18}F-FDG uptake.

TAC Induces Altered Myocardial Glucose Transporter Expression

Since ^{18}F-FDG uptake was more robust than expected from histologic evidence of leukocyte infiltration, we further investigated the efficacy of K/X to suppress glucose uptake after TAC. Blood glucose measurements at the time of acquisition confirmed hyperglycemia in both TAC and sham-operated animals (Fig. 4A), and was comparable between mice above and below the 10%ID/g threshold ($p=0.35$). Western immunoblotting demonstrated no difference in insulin-independent GLUT1 expression between TAC and sham operated animals in right or left ventricle. However, GLUT4 expression was elevated by 60% in TAC compared to sham animals, specifically in the left ventricle (Fig. 4B). Accordingly, metabolic changes of substrate utilization in pressure overloaded cardiomyocytes are a major contributor to the increased ^{18}F-FDG PET signal after TAC.

Elevated Myocardial ^{18}F-FDG-Uptake is Related to Early Functional Impairment

As both inflammation and metabolic changes may influence ventricular remodeling and cardiac function, we assessed the relationship between left ventricle ^{18}F-FDG signal and cardiac function. At 3d post-TAC a strong correlation to ejection fraction ($r = -0.75$, $p=0.01$), ESV ($r=0.75$, $p<0.01$) and EDV ($r=-0.67$, $p<0.05$) (Fig. 5A-C) was observed, which may suggest that animals with worse cardiac function exhibit ineffective cardiomyocyte suppression reflecting altered metabolic substrate utilization. This relationship was less prominent for LV mass and stroke volume at 3d (Fig. 5D), and all parameters at 7d (Supplemental Fig. 4).

DISCUSSION

Myocardial inflammation in cardiovascular disease is a powerful prognosticator of functional decline and an emerging therapeutic target. While strongly implicated in acute myocardial infarction and ischemic HF, inflammatory leukocyte contribution to non-ischemic pressure overload HF is less well characterized, owing in part to the challenge in non-invasive interrogation of local inflammation. Here, we evaluated the temporal relationship between ventricular geometric change, contractile function, and inflammation, and the capability of ^{18}F-FDG to non-invasively image inflammatory cell content. Histological analysis revealed mild diffuse inflammatory cell infiltration of the left ventricle early after pressure overload, but while ^{18}F-FDG uptake was increased, the intensity of the signal was disproportionate to the severity of inflammation. Tissue immunoblotting demonstrated a selective upregulation of GLUT4 in the overloaded left ventricle. The strain incurred by the myocardium during pressure overload renders K/X suppression of cardiomyocyte glucose transport ineffective, such that the ^{18}F-FDG signal early after TAC, while correlating with cardiac dysfunction, may partly reflect inflammation, but is probably dominated by metabolically compromised cardiomyocytes.

The role and time course of inflammatory cell invasion in myocardial infarction is well characterized, describing dynamic mobilization of leukocytes (*23*). By comparison, the role of inflammation in non-ischemic heart failure remains equivocal, though flow cytometry has identified inflammatory cell content in late-stage pressure overload heart failure (*10*). Previous studies demonstrate transient pro-inflammatory cytokines upregulation, and macrophage, but not granulocyte, recruitment, reaching maximum at 7d

after aortic constriction (*10,11*). Monocyte-derived cardiac macrophages are considered main contributors to adverse remodeling after TAC (*14*). In the present study, we observe modest diffuse CD68+ macrophage infiltration of the left ventricle beginning from 3d after TAC and persisting to 7d. Notably, MRI revealed elevated ventricle mass, dilatation, and contractile dysfunction in parallel to or preceding inflammatory cell infiltration. It is difficult to distinguish the role of inflammation in ventricular remodeling considering need for multiple timepoint tissue sampling.

Non-invasive interrogation of inflammatory leukocytes is therefore attractive to monitor disease progression. In several preclinical and clinical studies, ^{18}F-FDG uptake identifies inflammation in cardiovascular diseases e.g. acute MI (*19*), preferentially targeting metabolically active pro-inflammatory macrophages in cardiac tissue (*15,24*). However, the robust uptake of ^{18}F-FDG by cardiomyocytes limits the ability to specifically target inflammation in the heart. Previous studies established significantly higher ^{18}F-FDG uptake by the left ventricle within 24h of aortic constriction, which was effectively inhibited by beta blocker therapy (*18*). Elevated glucose utilization is associated with increased glucose-6 phosphate expression (*17*), which would be consistent with inability to suppress the cardiomyocyte 18F-FDG uptake in the present study. Moreover, the increased rate of glucose transport gradually increases over weeks of pressure overload (*17*), which may reflect the higher success of K/X cardiomyocyte suppression at the earlier timepoint (d3) of the current study. Accordingly, despite comparably elevated blood glucose levels following K/X anesthesia, upregulation of GLUT4 in the overloaded left ventricle prevents the normal suppression pattern. Notably, the chronic stages of pressure overload lead to regional hypometabolism, wherein the extent of myocardial metabolic defects correlates

with change in ventricular volume (*25*).As such, while diffuse inflammatory cells invade the myocardium in pressure overload, enhanced cardiomyocyte glucose utilization obscures the delineation of inflammation using ^{18}F-FDG. Of note, contractile function declined with rising ^{18}F-FDG uptake, consistent with altered metabolic substrate utilization in progressive remodeling. The interplay between inflammation and fibrosis believed to contribute to the progression of pressure overload heart failure (*26,27*), could be more effectively evaluated by specific inflammation agents (*28*).

Some limitations to the present study should be considered. Firstly, as we aimed to characterize the acute development of inflammation in pressure overload, we did not assess the long-term functional outcome. We were primarily interested in the acute stage of disease, when inflammation is thought to predicate remodeling and fibrosis prior to terminal heart failure. The rapid change in ventricle geometry and decline in contractile function in parallel with inflammation and metabolic perturbation suggests we have captured active stage of disease. Secondly, as we used separate camera systems, we could not assess cardiac function and ^{18}F-FDG distribution on the same day, such that correlations may be imprecise. Despite gradual increase in the ventricle volumes and mass, the ejection fraction remains relatively consistent from 2d to 8d, supporting the correlation between PET and MRI measurements. Finally, we evaluated only K/X anesthesia as a means of suppressing cardiomyocyte ^{18}F-FDG uptake. Earlier studies indicate that continuous administration of propranolol prevents glucose hypermetabolism (*18*). Because the sympathetic nervous system is also known to modulate ventricular remodeling and inflammatory leukocyte mobilization (*29*), and the temporal pattern of leukocyte infiltration is poorly characterized, we focused specifically on K/X suppression.

In conclusion, TAC induces rapid changes in left ventricle geometry and contractile function with a parallel modest increase in acute inflammatory cell infiltration. ^{18}F-FDG imaging cannot effectively resolve inflammatory cells in the presence of extensive cardiomyocyte metabolic remodeling, as in pressure-overload heart failure. A more selective molecular tracer targeting inflammation may provide a clearer illustration of the local inflammatory response and its contribution to pathogenesis.

ACKNOWLEDGMENTS

This study was partly supported by the German Research Foundation (DFG, Clinical Research Group KFO311, Excellence Cluster REBIRTH-2, and research grant TH2161/1-1). The authors thank the Preclinical Molecular Imaging and the Small Animal MRI Centre for their technical assistance with these experiments.

Disclosure

No potential conflicts of interest relevant to this article exist.

KEY POINTS

QUESTION: Can 18F-FDG imaging identify inflammatory leukocyte infiltration of the myocardium early in pressure overload-induced heart failure?

PERTINENT FINDINGS: Cardiac 18F-FDG uptake is elevated after transverse aortic constriction, but is disproportionate to the diffuse infiltration of inflammatory macrophages due to increased glucose metabolism by the overloaded heart.

IMPLICATIONS FOR PATIENT CARE: Assessment of inflammation with ^{18}F-FDG may be imprecise in non-ischemic heart failure, necessitating more specific imaging agents.

REFERENCES

1. Savarese G, Lund LH. Global Public Health Burden of Heart Failure. *Card Fail Rev.* 2017;3:7-11.

2. Ponikowski P, Voors AA, Anker SD, et al. 2016 ESC Guidelines for the diagnosis and treatment of acute and chronic heart failure: The Task Force for the diagnosis and treatment of acute and chronic heart failure of the European Society of Cardiology (ESC)Developed with the special contribution of the Heart Failure Association (HFA) of the ESC. *Eur Heart J.* 2016;37:2129-2200.

3. Bengel FM, George RT, Schuleri KH, Lardo AC, Wollert KC. Image-guided therapies for myocardial repair: concepts and practical implementation. *Eur Heart J Cardiovasc Imaging.* 2013;14:741-751.

4. Hofmann U, Frantz S. How can we cure a heart "in flame"? A translational view on inflammation in heart failure. *Basic Res Cardiol.* 2013;108:356.

5. Ammirati E, Cannistraci CV, Cristell NA, et al. Identification and predictive value of interleukin-6+ interleukin-10+ and interleukin-6- interleukin-10+ cytokine patterns in ST-elevation acute myocardial infarction. *Circ Res.* 2012;111:1336-1348.

6. Barron HV, Harr SD, Radford MJ, Wang Y, Krumholz HM. The association between white blood cell count and acute myocardial infarction mortality in patients > or =65 years of age: findings from the cooperative cardiovascular project. *J Am Coll Cardiol.* 2001;38:1654-1661.

7. Bozkurt B, Torre-Amione G, Warren MS, et al. Results of targeted anti-tumor necrosis factor therapy with etanercept (ENBREL) in patients with advanced heart failure. *Circulation.* 2001;103:1044-1047.

8. Rischpler C, Dirschinger RJ, Nekolla SG, et al. Prospective Evaluation of 18F-Fluorodeoxyglucose Uptake in Postischemic Myocardium by Simultaneous Positron Emission Tomography/Magnetic Resonance Imaging as a Prognostic Marker of Functional Outcome. *Circ Cardiovasc Imaging.* 2016;9:e004316.

9. Brenes-Castro D, Castillo EC, Vazquez-Garza E, Torre-Amione G, Garcia-Rivas G. Temporal Frame of Immune Cell Infiltration during Heart Failure Establishment: Lessons from Animal Models. *Int J Mol Sci.* 2018;19.

10. Patel B, Ismahil MA, Hamid T, Bansal SS, Prabhu SD. Mononuclear Phagocytes Are Dispensable for Cardiac Remodeling in Established Pressure-Overload Heart Failure. *PLoS One.* 2017;12:e0170781.

11. Weisheit C, Zhang Y, Faron A, et al. Ly6C(low) and not Ly6C(high) macrophages accumulate first in the heart in a model of murine pressure-overload. *PLoS One.* 2014;9:e112710.

12. Xia Y, Lee K, Li N, Corbett D, Mendoza L, Frangogiannis NG. Characterization of the inflammatory and fibrotic response in a mouse model of cardiac pressure overload. *Histochem Cell Biol.* 2009;131:471-481.

13. Chen B, Frangogiannis NG. The Role of Macrophages in Nonischemic Heart Failure. *JACC Basic Transl Sci.* 2018;3:245-248.

14. Patel B, Bansal SS, Ismahil MA, et al. CCR2(+) Monocyte-Derived Infiltrating Macrophages Are Required for Adverse Cardiac Remodeling During Pressure Overload. *JACC Basic Transl Sci.* 2018;3:230-244.

15. Satomi T, Ogawa M, Mori I, et al. Comparison of contrast agents for atherosclerosis imaging using cultured macrophages: FDG versus ultrasmall superparamagnetic iron oxide. *J Nucl Med.* 2013;54:999-1004.

16. Young LH, Russell RR, 3rd, Yin R, et al. Regulation of myocardial glucose uptake and transport during ischemia and energetic stress. *Am J Cardiol.* 1999;83:25H-30H.

17. Sen S, Kundu BK, Wu HC, et al. Glucose regulation of load-induced mTOR signaling and ER stress in mammalian heart. *J Am Heart Assoc.* 2013;2:e004796.

18. Zhong M, Alonso CE, Taegtmeyer H, Kundu BK. Quantitative PET imaging detects early metabolic remodeling in a mouse model of pressure-overload left ventricular hypertrophy in vivo. *J Nucl Med.* 2013;54:609-615.

19. Thackeray JT, Bengel FM. Molecular Imaging of Myocardial Inflammation With Positron Emission Tomography Post-Ischemia: A Determinant of Subsequent Remodeling or Recovery. *JACC Cardiovasc Imaging.* 2018;11:1340-1355.

20. Tarnavski O, McMullen JR, Schinke M, Nie Q, Kong S, Izumo S. Mouse cardiac surgery: comprehensive techniques for the generation of mouse models of human diseases and their application for genomic studies. *Physiol Genomics.* 2004;16:349-360.

21. Thackeray JT, Bankstahl JP, Wang Y, Wollert KC, Bengel FM. Clinically relevant strategies for lowering cardiomyocyte glucose uptake for 18F-FDG imaging of myocardial inflammation in mice. *Eur J Nucl Med Mol Imaging.* 2015;42:771-780.

22. Zuo Z, Subgang A, Abaei A, et al. Assessment of Longitudinal Reproducibility of Mice LV Function Parameters at 11.7 T Derived from Self-Gated CINE MRI. *Biomed Res Int.* 2017;2017:8392952.

23. Frangogiannis NG, Smith CW, Entman ML. The inflammatory response in myocardial infarction. *Cardiovasc Res.* 2002;53:31-47.

24. Lee WW, Marinelli B, van der Laan AM, et al. PET/MRI of inflammation in myocardial infarction. *J Am Coll Cardiol.* 2012;59:153-163.

25. Todica A, Beetz NL, Gunther L, et al. Monitoring of Cardiac Remodeling in a Mouse Model of Pressure-Overload Left Ventricular Hypertrophy with [(18)F]FDG MicroPET. *Mol Imaging Biol.* 2018;20:268-274.

26. Kallikourdis M, Martini E, Carullo P, et al. T cell costimulation blockade blunts pressure overload-induced heart failure. *Nat Commun.* 2017;8:14680.

27. Patel VB, Bodiga S, Fan D, et al. Cardioprotective effects mediated by angiotensin II type 1 receptor blockade and enhancing angiotensin 1-7 in experimental heart failure in angiotensin-converting enzyme 2-null mice. *Hypertension.* 2012;59:1195-1203.

28. Thackeray JT, Derlin T, Haghikia A, et al. Molecular Imaging of the Chemokine Receptor CXCR4 After Acute Myocardial Infarction. *JACC Cardiovasc Imaging.* 2015;8:1417-1426.

29. Dutta P, Courties G, Wei Y, et al. Myocardial infarction accelerates atherosclerosis. *Nature.* 2012;487:325-329.

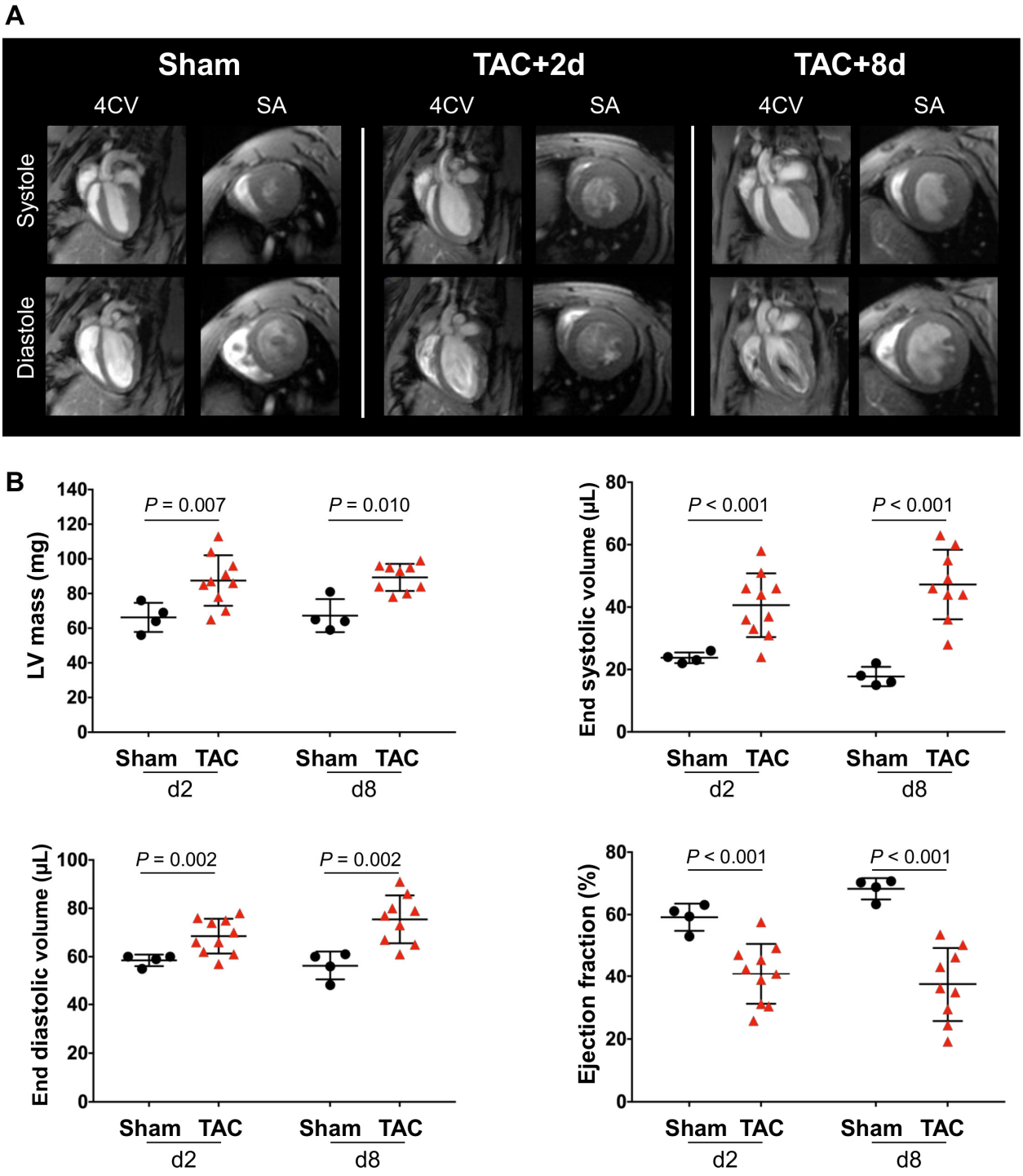

Figure 1. (A) Representative cardiac 4-chamber view (4CV) and short axis (SA) images show elevated heart volume and dilatation of the left ventricle after TAC. (B) Quantitative functional analysis of left ventricular mass (upper left), end systolic volume (upper right), end diastolic volume (lower left) and ejection fraction (lower right).

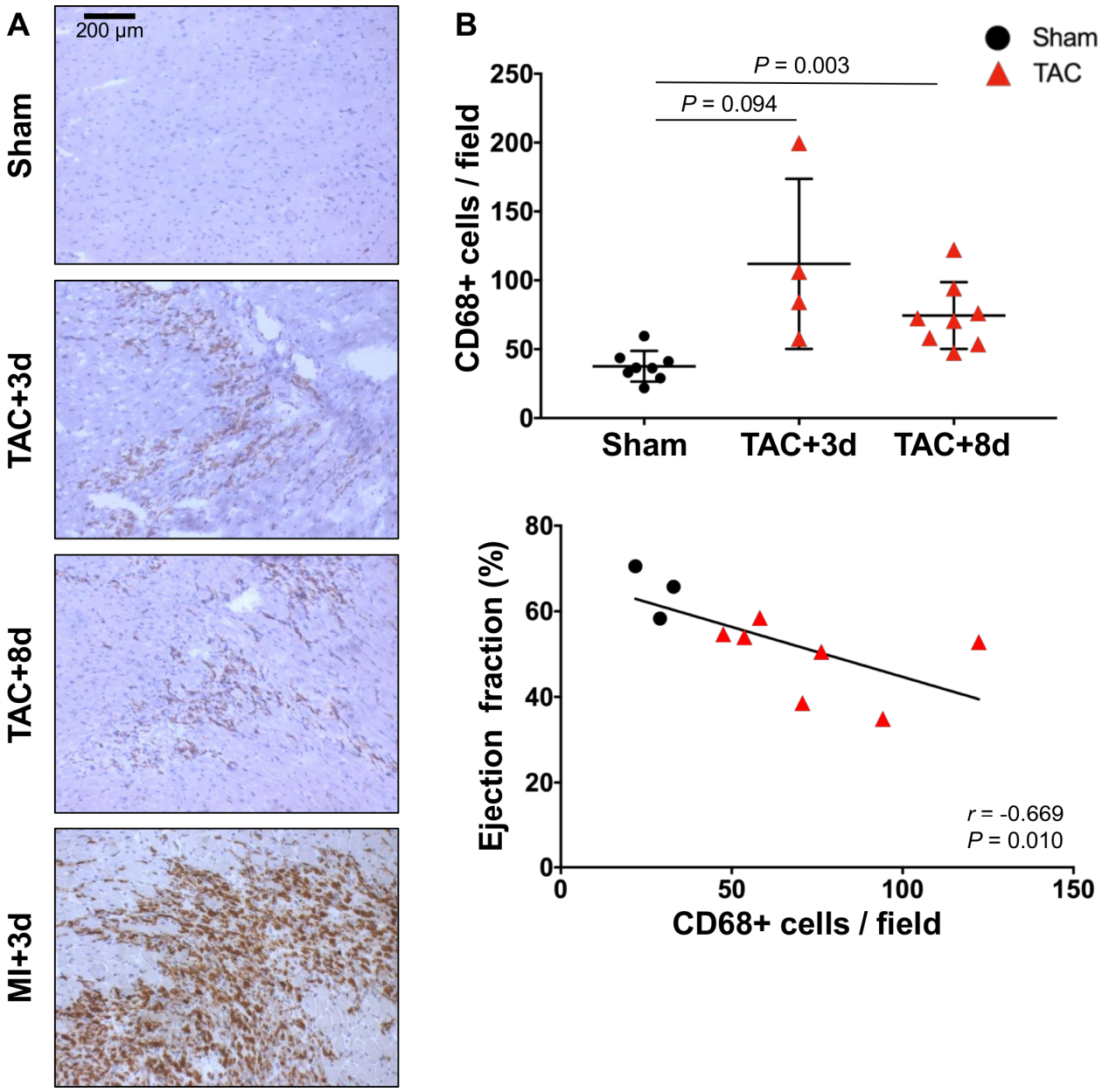

Figure 2. (A) CD68 immunostaining of representative long axis sections at 3d and 8d after TAC and 3d after MI. (B) Quantitative analysis of stained sections shows elevation of CD68+ cells/field 3d and 8d after TAC (top) which inversely correlates to impaired ejection fraction at 8d after TAC (lower).

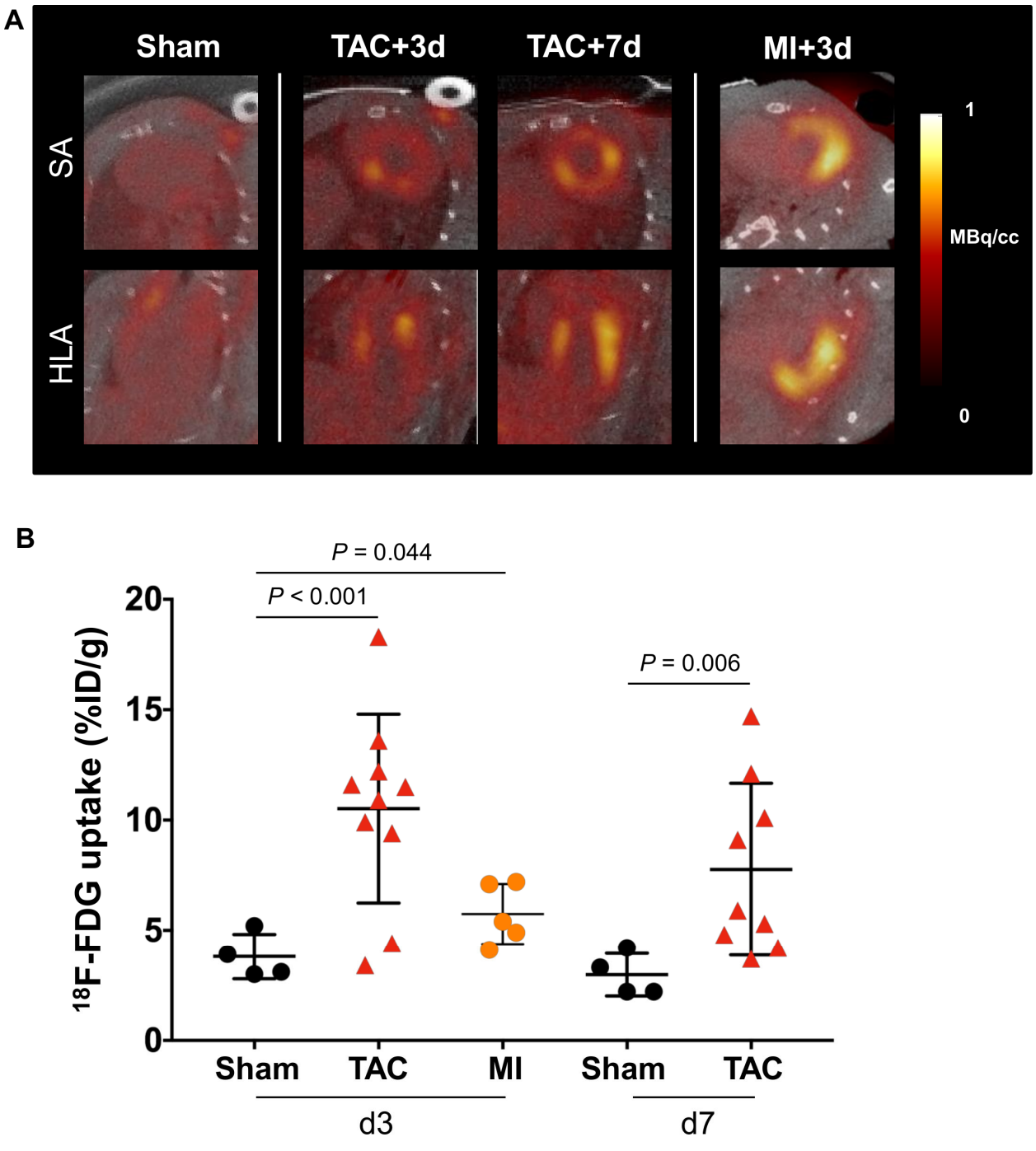

Figure 3. (A) Representative ^{18}F-FDG short axis (SA) and horizontal long axis (HLA) images under effective ketamine-xylazine suppression of cardiomyocyte glucose uptake displays global myocardial inflammation at 3d and 7d after TAC. Elevated ^{18}F-FDG uptake is localized to the infarct territory after MI. (B) Semi-quantitative assessment of ^{18}F-FDG mean percent injected dose per gram (%ID/g).

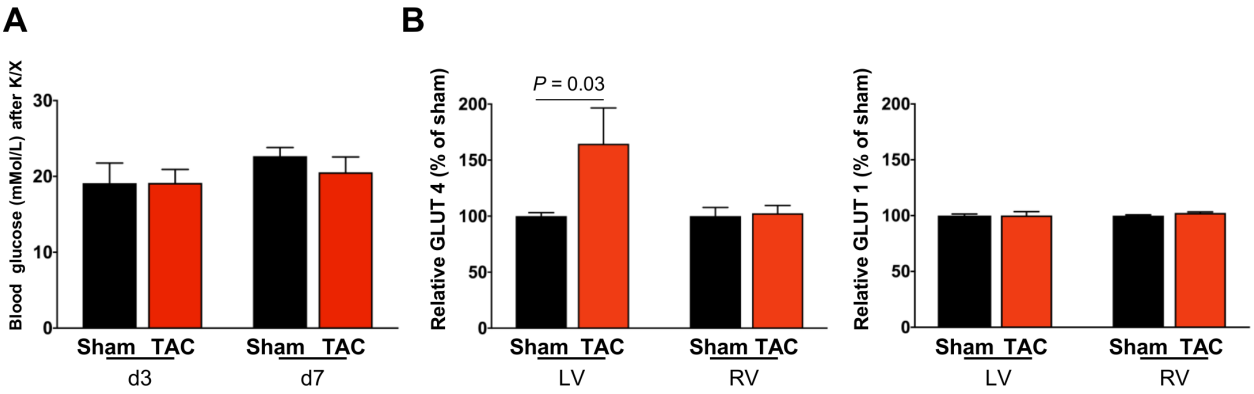

Figure 4. (A) Blood glucose levels are comparably elevated under ketamine-xylazine anesthesia in TAC and sham mice. (B) Quantification of Western immunoblots display elevated GLUT4 expression in left ventricle (LV) but not right ventricle (RV) after cardiac pressure overload, and no change in insulin-independent GLUT1 at 8d after TAC.

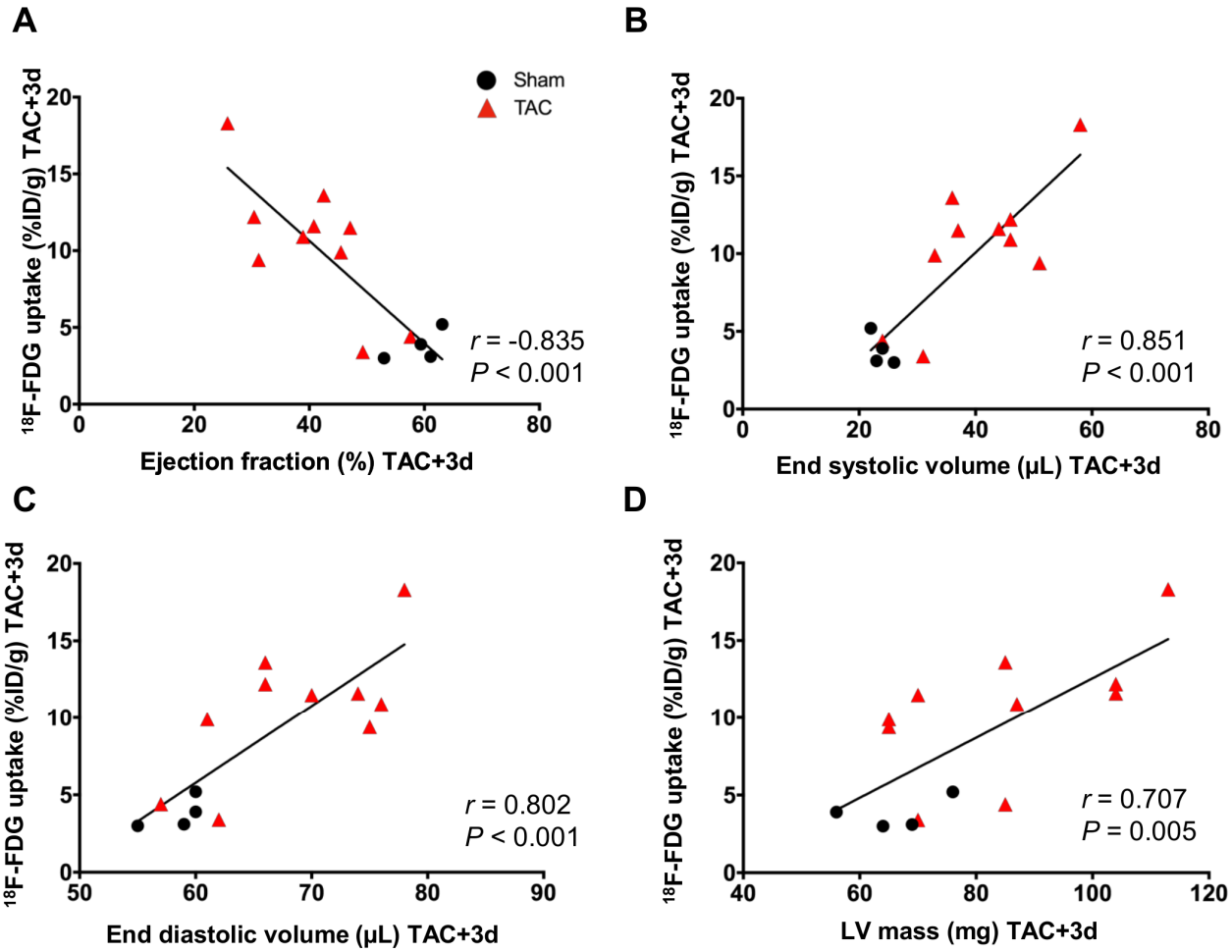

Figure 5. Correlation of cardiac geometry and function with 18F-FDG accumulation in left ventricle at 3d after TAC, displaying inverse correlation to (A) ejection fraction, and direct correlation to (B) left ventricular end systolic volume, (C) end diastolic volume and (D) left ventricular mass.

Supplemental Methods

Cardiac MRI Acquisition. Mice (TAC n=10, sham n=4) underwent MRI at 2d and 8d after surgery using a 7 Tesla small animal MRI system (Pharmascan 70/16, Bruker BioSpin GmbH, Ettlingen, Germany; Software ParaVision 6.0.1). Cardiac function and geometry were evaluated by using a navigator-based self-gated cine MRI sequence (IntraGate FLASH, Bruker Biospin, Ettlingen, Germany) as described previously (*15*). A 72-mm-diameter volume transmit coil (T11070 89/72 Quad to AD, Bruker BioSpin MRI GmbH) was used in combination with an anatomically shaped four-element mouse cardiac phased-array surface receive coil (T20027V3, Bruker BioSpin MRI GmbH). The animals were positioned prone and body temperature was maintained by a water-heated system during examination. All scans were performed in isoflurane inhalation anesthesia (3% induction, 2% maintenance). Respiration rate was monitored and kept between 50-60 breaths per minute.

Cine images were acquired in 4 chamber view to visualize the aortic banding and short-axis (SA) orientation that covered the whole left ventricle (LV). Sequence parameters (SA) were: field of view (FOV) 25×25mm, matrix 196×196, slice thickness 0.9mm, slice distance 0.9mm, repetition time (TR) 84.64ms, echo time (TE) 1.84ms, flip angle 45°, number of reconstructed phases 24.

MRI Image Analysis. Image analysis was performed with CVI (Vers. 5.3.6 Circle Cardiovascular Imaging, Calgary, Alberta) to determine ventricle volumes and assess heart function. Endocardial and epicardial contours were defined on short axis sections and used to calculate ventricular mass at end systole and end diastole; ejection fraction was calculated from endocardial volumes.

PET image reconstruction and analysis. All PET images were reconstructed to a $128 \times 128 \times 159$ image matrix ($0.78 \times 0.78 \times 0.80$ mm) using an OSEM3D/MAP algorithm

($\beta = 0.01$, 2 OSEM iterations in 16 subsets, 18 MAP iterations) with scanner-applied decay- and scatter-correction. A ^{57}Co transmission scan was used for attenuation correction (*14*).

Western Immunoblotting. Hearts were excised and dissected to separate the left and right ventricle, then flash frozen under liquid nitrogen. Tissue was stored at -80°C until use. Western immunoblotting was performed as described previously (*17*). Briefly, tissue samples were homogenized in lysis buffer separated by gel electrophoresis. Primary antibodies were mouse monoclonal anti-glucose transporter GLUT1 (SPM498, 1/5000), mouse monoclonal anti-glucose transporter GLUT4 (ab65267, 1μg/ml) (Abcam). Secondary antibody was rabbit polyclonal anti-mouse IgG conjugated to horseradish peroxidase (Abcam). Immunoblots were analysed by chemiluminescence and integrated density values normalized to β-actin loading control were compared between groups.

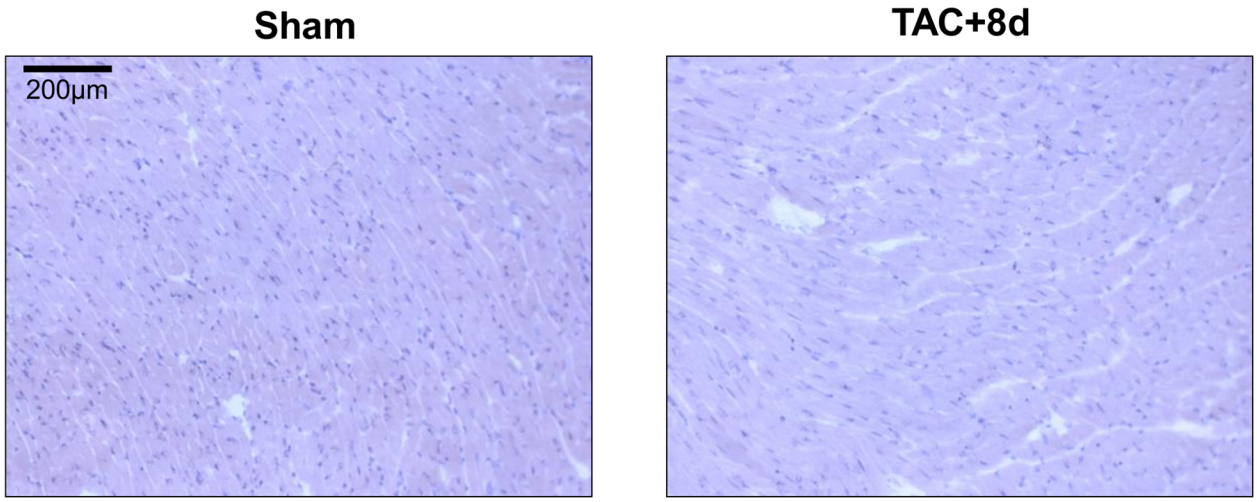

Supplemental Figure 1. Immunohistologic Ly6G+ staining of representative long axis sections demonstrates no change in Ly6G-positive cells in left ventricular myocardium 8d after TAC compared to sham.

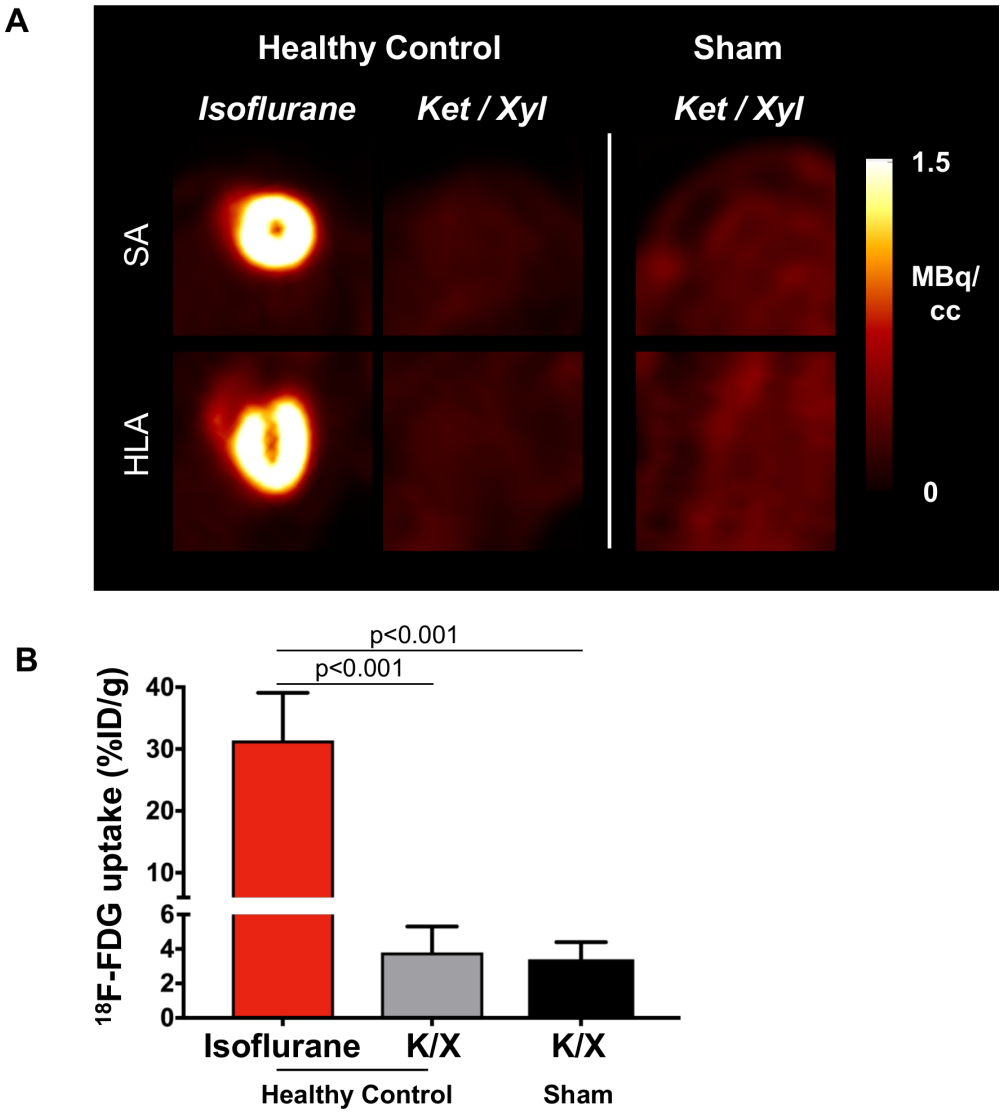

Supplemental Figure 2. Ketamine-xylazine (K/X) anesthesia suppresses cardiomyocyte glucose uptake effectively in healthy control and sham mice

(A) Robust ^{18}F-FDG uptake in healthy myocardium under isoflurane anesthesia without K/X suppression. K/X suppression of cardiomyocyte ^{18}F-FDG uptake lowered tracer uptake in healthy control mice to background levels, comparable to sham-operated animals. (B) Quantitative ^{18}F-FDG signal shows elevation in healthy mice under isoflurane anesthesia (31.4±7.7 %ID/g, n=6). Signal under K/X anesthesia is comparable in healthy control mice (3.8 ±.1.5 %ID/g, n=5) and sham (3.4 ± 1.0 %ID/g, n=8).

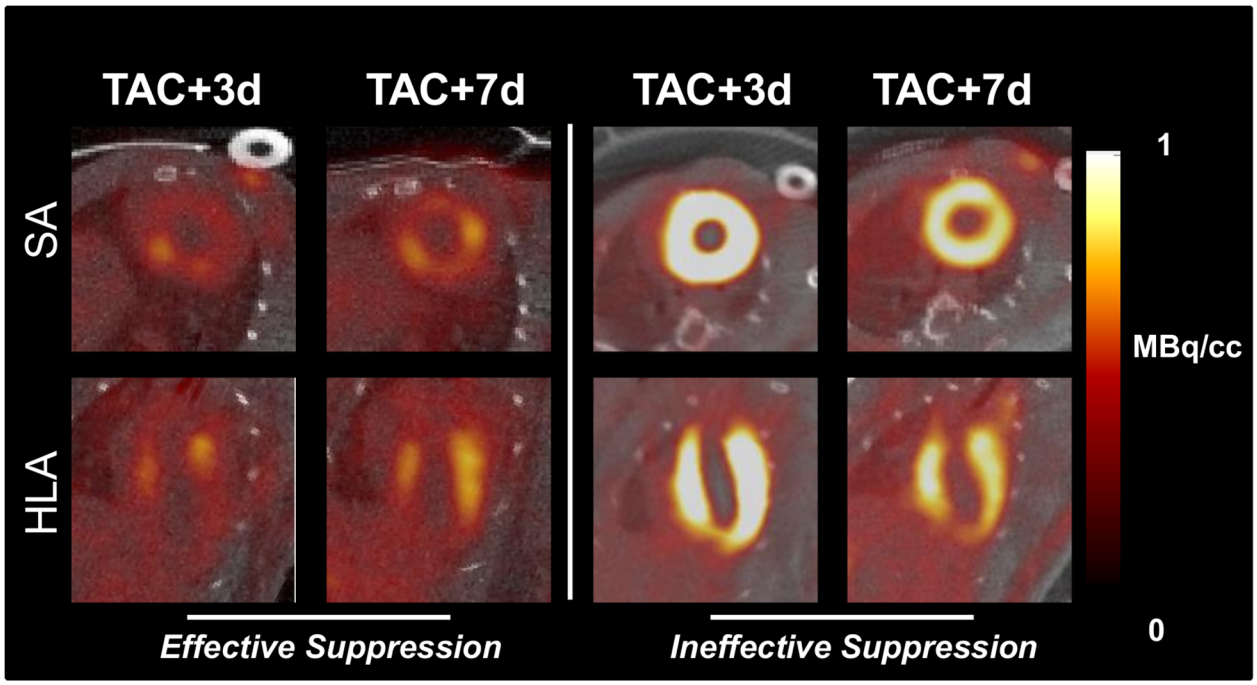

Supplemental Figure 3. Cardiac functional parameter are not related to elevated ^{18}F-FDG signal at 8d after surgery (A) Correlation of stroke volume (µL) at d2 and d8 to ^{18}F-FDG signal. (B) Elevated left ventricular end systolic volumes (µL), end diastolic volumes (µL), left ventricular mass and ejection fraction (%) at 8d do not correlate to ^{18}F-FDG signal at 7d.

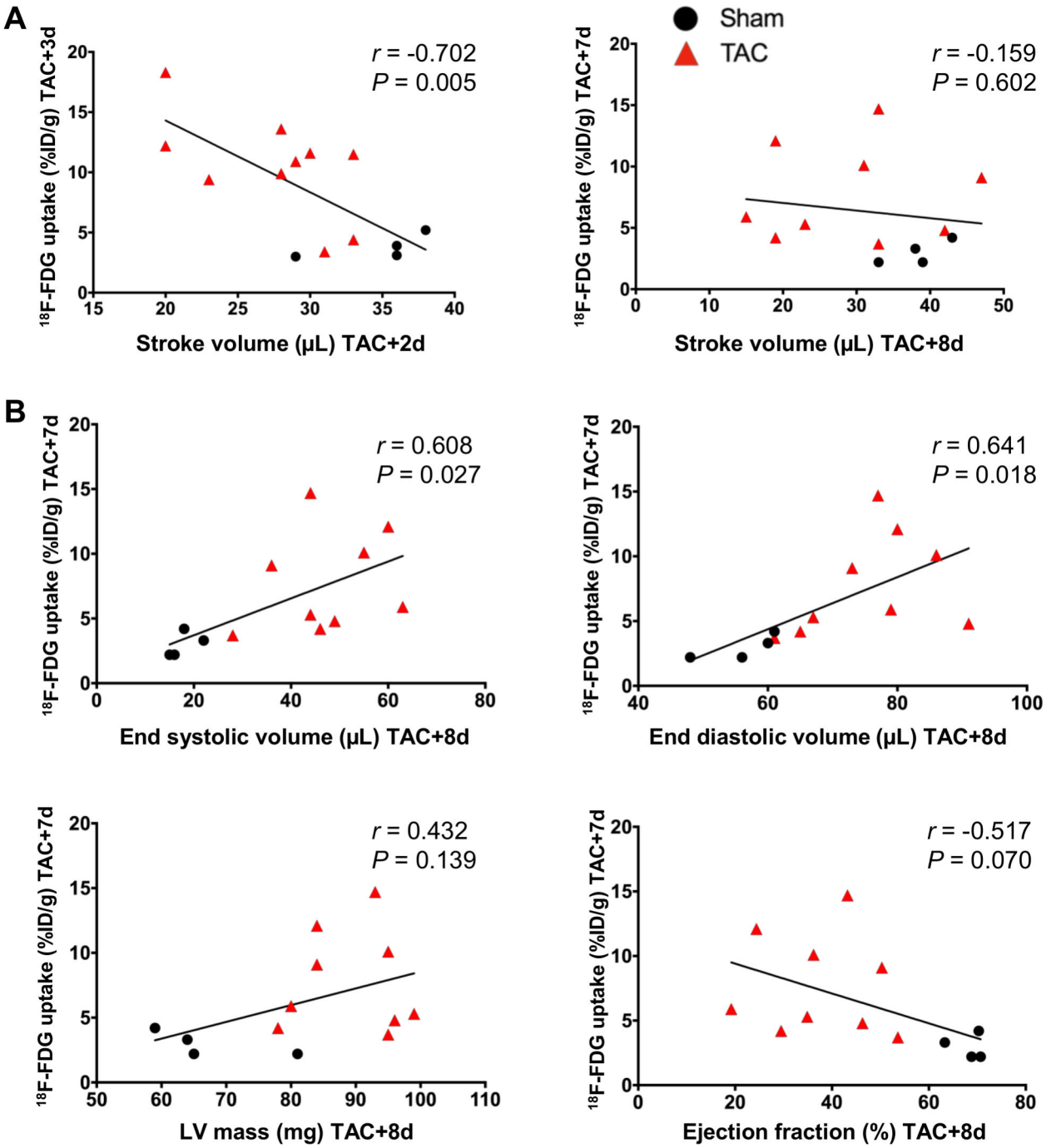

Supplemental Figure 4. Ineffective K/X suppression of cardiomyocyte glucose uptake visualizes altered cardiac glucose metabolism in response to cardiac pressure overload

Diffuse ^{18}F-FDG signal in SA and HLA images under effective K/X suppression of cardiomyocyte glucose uptake reflects global myocardial inflammation, whereas robust ^{18}F-FDG signal in the LV shows insufficient suppression of cardiomyocyte glucose uptake.